Int J Adv Manuf Technol (2017) 93:407–422
DOI 10.1007/s00170-016-9698-6

ORIGINAL ARTICLE

Solid silicon microneedles for drug delivery applications

S. Pradeep Narayanan [1] · **S. Raghavan** [1]

Received: 18 September 2016 / Accepted: 3 November 2016 / Published online: 27 December 2016
© Springer-Verlag London 2016

Abstract In this work, solid silicon (Si) microneedles with a higher aspect ratio and sharper tips are fabricated. Tetramethylammonium Hydroxide (TMAH) etching factors have been optimized and used to fabricate long and tapered microneedles. The needles thus fabricated are found to be suitable for transdermal drug delivery applications. The optimized etching factors include varying the concentration of TMAH, etching time, etching rates, temperature, and window size of optical mask. It is found that by increasing the window size, the etch rates in both vertical and lateral directions increase extensively. However, on increasing the temperature beyond 90 °C, etching becomes rapid and uncontrollable. In order to obtain microneedles with high aspect ratio, sample placement in the glass boat of TMAH setup and TMAH concentration should be manipulated to attain a higher etch rate in vertical direction compared to the lateral one. Solid silicon microneedles with an average height of 158 μm, base width of 110.5 μm, aspect ratio of 1.43, tip angle of 19.4° and tip diameter of 0.40 μm are successfully fabricated. A microhardness value of 44.4 (HRC) was obtained for the fabricated Si microneedles. This is 52.2 times higher than the skin Ultimate Tensile Strength (UTS), which makes insertion of microneedles through the skin safer and easier without any breakage.

Keywords Bio-MEMS · Drug delivery · Silicon microneedles · Transdermal patch

✉ S. Pradeep Narayanan
narenpradeep@gmail.com

[1] Department of Electronics and Communication Engineering, National Institute of Technology, Tiruchirappalli, Tamil Nadu, India

1 Introduction

Pills and injections are the existing ways of drug delivery for pain curing, which in turn cause adverse side effects such as itching, irritation, Gastrointestinal (GI) tract from the mouth to colon. This seems to be the most significant problem that arises in the administration of drug delivery system which needs a solution. Among various kinds of effective drug delivery systems for human body, Transdermal Drug Delivery System (TDDS) has been progressively used since early 1990s [1]. Transdermal patches are the first generation and first outcome in clinical use of transdermal delivery systems. The second-generation transdermal systems such as chemical enhancers, iontophoresis, and non-cavitational ultrasound, identified the need in enhancement of skin permeability. This has lead to an enhancement in the scope of transdermal drugs [2, 3]. To deliver macromolecules like drugs by crossing the effective Stratum Corneum (SC) barrier across the human skin to reach the target desirably, third-generation transdermal systems such as combination of chemical enhancers, biochemical enhancers, electroporation, cavitational ultrasound, thermal ablation, microdermabrasion, and microneedles are being used [4, 5].

Depending upon the molecular weight, dosage level, lipophilicity, metabolizing propensity, and drug administer efficiency, appropriate selection of transdermal technique is made. Microneedles are the one which solves the above problem with no side effects and looks exactly like a traditional hypodermic needle, but in micron size by coating a drug or vaccine at their tips [6–8]. The length may vary from 1 to 100 μm whereas diameter is around 1 μm. To deliver the drugs in a precise place, without causing any pain microneedles are found to play a phenomenal role. It precipitates drug metabolization from the first-pass effect which have been a concern in an oral drug delivery [1, 9]. On the other side, hypodermic

needle has drawbacks like a requirement of a professional person to administer drugs, production of more medical waste, less preference from patients due to the associated pain and the risk of disease diffusion [2]. In the recent decade, microneedles are being used in clinical trials to deliver macromolecules drugs like hormones, insulin and vaccines [10, 11].

The keratin-filled SC layer is minimally poked by the microneedles and then create a microscale hole in epidermis to transport the drugs into the dermal-epidermal junction. In addition, transdermal drug administration using microneedles has four different approaches, namely “Poke and Patch,” “Coat and Poke,” “Poke and Release,” and “Poke and Flow” [12]. The first three approaches corresponds to solid microneedles for transdermal drug delivery applications. The poke and patch replicates poking the SC layer up to dermal-epidermal junction without any pain. Then, it releases the drug loaded as a patch through micropores created on the skin. In coat and poke approach, drugs are first coated in the needles and the detachment of coated drug would take place after it pokes the skin [6, 13]. Dissolving microneedles will use the poke and release approach for the diffusion of drugs though the pores. It is mainly made using biodegradable polymers to dissolve completely and release the drug into the skin [14]. The last approach, poke and flow is mainly used with hollow microneedles where the drug flows through the lumen or bore of the microneedles after it has poked the SC layer of the skin [15]. Not only in the diagnosis of TDDS, microneedle functionalities are extended to therapies as well. The quantity of drugs being in micrograms and microliters, microneedles does not cause any pain to the nerves.

Initially, silicon was the only suitable material chosen for the fabrication process to get sharper tips with further improvement in the skin permittivity. Research on materials, made an establishment for silicon dioxide, metals, glass, polymers, metal-coated silicon, biodegradable materials, and many others as an alternate material [2]. Use of these material microneedle-based transdermal patches have been made without puncturing the nerves, but by crossing the SC layer of the skin to influence the dermal-epidermal junction [16–18]. Human skin is made up of three major layers, viz SC layer with 20–30 μm thickness, the Viable Epidermis (VE) layer with 50–100 μm thickness. This layer lies on the top of dermis layer, i.e., the third layer. In dermis layer, considerable quantity of vascular loops exist and that makes delivering drugs to disperse thoroughly to reach a medicament level. Major design parameters are easy tip penetration, adequate mechanical strength to diffuse across the skin and a significant base of the microneedles to avoid needle breakages during penetration.

Silicon microneedles are mainly classified into two types, namely solid and hollow. It may be either in-plane or out-of-plane based on the fabrication process with various types like straight, bent, etc. [19–21]. Diffusion rate dependency and increase in skin permeability are the key factors to transfer the drug through silicon microneedles. This is achieved either by loading drug in lumen if it is hollow type or by coating the drug at the tip if it is a solid one [22, 23]. For a controlled and timely release of drugs into the body, array of solid silicon microneedles could be used. For this, a combo of micropumps or simple diffusion system is used either to deliver drugs or to extract any fluids like blood and glucose measurements in a microliter volume. Biocompatibility is the prime factor to be considered during solid silicon microneedles design. It is being improved mainly by coating some metals at the tips while delivering drugs via the skin [24–27].

Hashmi et al. fabricated the initial solid silicon microneedle array using wet etching, i.e., KOH (Potassium Hydroxide) [28]. They used the mask layer as silicon dioxide and microneedles formed here were in a pyramid structure. They have been stacked which has less than 1 μm of tip diameter. Due to comparatively large body and base of the needles, it causes possible skin tissue damage during penetration. Shilpa kaushik et al. [29] demonstrated that an area of 3-mm by 3-mm size nearly 400 microneedles in an array is used to deliver drug molecules. It targets the individual cells by piercing the outer layer of the skin. Many technologies are established to make microneedles more biocompatible using metals and polymers, where recent microneedle-based transdermal patch will also become biodegradable in nature too. Using microfabrication and lithography techniques, plenty of research is in progress to produce huge numbers of solid silicon microneedles [30–34].

Li Wei–Ze et al. [35] and Harvinder S. Gill et al. [36] have discussed the flat tip type solid in-plane microneedles. However, most of the microneedles with flat tips could not solve the wastage of drugs while penetrating inside the skin during drug delivery. Jing Ji et al. [37] clearly explained about obtaining porous and biodegradable tips of solid silicon microneedle arrays by introducing a feasible fabrication process. Higher capacity of drugs can be stored in the pores at the tips due to its porous nature. In order to avoid needle damages and blockage during skin penetration and to reduce insertion force of microneedles, various shapes of solid Si microneedles have been fabricated and reported in literatures. Table 1 provides the various dimensions of fabricated solid Si microneedles. Recent days, large number of research groups have started focusing on dissolving polymer microneedles to increase the efficiency and biocompatibility, while delivering drugs [40–43]. For a compact drug delivery system, dissolving polymer microneedles perfectly matched for its operation both as drug delivery device and drug construction independently [44–47]. Hence, we enhance the available fabrication of silicon etching technique with minimum process steps and to achieve a cost effective device in the transdermal drug delivery system.

Table 1 Typical properties of the solid Si microneedles

Typical parameters (μm)	Kaushik et al. [29]	Henry et al. [6]	McAllister et al. [18]	Wilke et al. [38]	Hanein et al. [39]	H. S. Gill et al. [36]
Microneedle height	150 μm	~ 150 μm	25 μm	400 μm (Dry etching) 280 μm (Wet etching)	230 μm	480 to 1450 μm
Base diameter	80 μm	–	15 μm	200 μm	70 μm	–
Microneedle tip diameter	1 μm (radius of curvature)	–	less than 1 μm	less than 1 μm wide	200 nm wide	–

Even now, silicon-based microneedles are gathering numerous improvements because of their promptness to get it incorporated with other devices like silicon-based Bio-MEMS sensors, actuators, etc. Motivated by the compatibility of Si as an essential material and the need to construct more preferentially shaped microneedles for pain less transdermal drug delivery, this paper optimizes and characterizes Tetramethylammonium Hydroxide (TMAH) etching. Aspect ratio, mechanical strength, and fracture strength are the most important features for the prosperous drug delivery through microneedles. Aspect ratio is the needle height to base width ratio, micron hole created in the skin during penetration shows the mechanical strength of the needles and needle fails via fracture to its stress applied, respectively.

With this aim, we attempted to discuss the design, fabrication, and characterization of solid silicon microneedles having a high aspect ratio by using single step lithography and anisotropic wet etching (TMAH) process. The key factor considered here is mainly to increase the insertion length of the microneedles with sharper tips and unique shape, so that it can reach the effective depth region of TDDS. The optical mask window size, composition of TMAH, etching rates both in lateral and vertical directions and the etching temperature to achieve the microneedles structure are studied and characterized. We also studied the optical properties and mechanical strength of the microneedles before it is being used to deliver the coated drug. Many factors involved in TMAH etching increase the complexity to attain a repeatable etch results. We try to illustrate TMAH etching factors to obtain repeatable process for ideal fabrication of solid silicon microneedles.

The uniformity and thickness of the SiO_2 layer are studied using ellipsometer and optical spectroscopy. Elemental analysis is made for solid silicon microneedles using Energy-Dispersive X-ray (EDX) spectroscopy attached with a Field Emission-Scanning Electron Microscope (FE–SEM). The structural and optical properties are studied by Fourier Transform Infrared (FTIR) and Ultraviolet-Visible-Near-Infrared (UV-Vis-NIR) spectroscopy techniques. The aspect ratio of microneedles is considered to be the prime factor during fabrication. The hardness of the solid silicon microneedles is tested using the Vickers hardness test.

2 Experimental section

2.1 Design

As described earlier, human skin has mainly three layers, where the structure includes feasible epidermis in it. While designing microneedles care has been taken, so as to penetrate the feasible epidermis. It's length should be longer than that used to deliver a drug via a skin, so as to cross the feasible epidermis. To achieve the desired shape, these are the important phenomenon to be considered both in design and fabrication of solid silicon microneedles. The Miller index (h k l) of silicon has several types, (100), (111), (110) and so on. Si (100) wafer was chosen here, along with the different concentration of TMAH to optimize and achieve a proper V-groove using anisotropic wet etching. The primary reasons are that the angle between the (100) and (111) is 54.70° and the etching rate of (100) > (111) > (110).

$$\frac{x}{(w+2t)/2} = \tan 54.7° \quad (1)$$

V-groove dimensions are designed by using Eq. (1), where w is the width of expose square window, t is the thickness of the oxide layer and by taking undercut into account, it is easy to obtain the depth, x, as shown in Fig. 1a [48]. While etching, the crystal orientation of silicon has diverse indices and the corner compensation which gives four (111) planes with 54.7° between the etched face and the horizontal surface as shown in Fig. 1b [48].

2.2 Fabrication process of solid Si microneedles

Photolithography and micromachining techniques are incorporated for the realization of microneedles. Figure 2 shows the optical mask window size used for patterning Positive Photoresist (PPR) and to fabricate solid silicon microneedles. Figure 3 shows the graphical form of the fabrication process steps involved. Initially, a Single Side Polished (SSP) 4″ inch P-type Si wafer with (100) crystallographic orientation was cleaned using standard Radio Corporation of America (RCA) cleaning process for 30 min (step 1 in Fig. 3). The cleaned wafer was oxidized, i.e., SiO_2 layer created on both sides of the wafer using Ultech Low Temperature Oxide (LTO) furnace (step 2

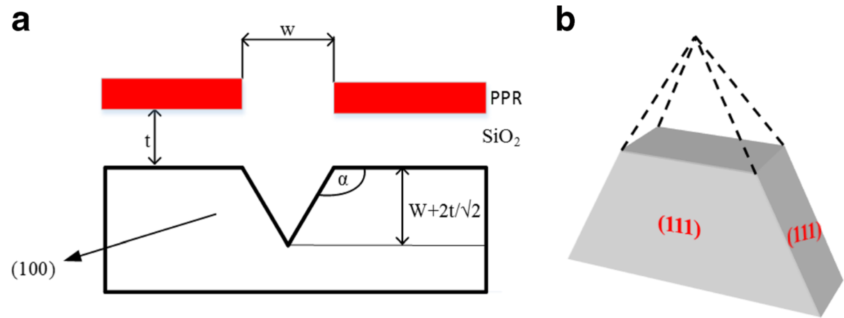

Fig. 1 **a** V-groove dimension. **b** Schematic representation of silicon by wet etching

in Fig. 3). The wafer was coated with PPR S1813 on both sides, for which it was spun at 3000 RPM for 30 s with 15 s prespin at 300 RPM, to get 2 μm thickness approximately (step 3 in Fig. 3). Si wafer was prebaked for 3 min at 90 °C and were aligned using the optical mask with an array of 180 μm window size, i.e., solid dark squares as shown in Fig. 2. Ultra-Violet (UV) is exposed using Double Side Aligner (DSA)—EVG 620 Optical Lithography, developed, and hard baked again at 90 °C for 3 min to solidify the cross-linking pattern over photoresist (step 4 & 5 in Fig. 3). Lateral and vertical gaps between the squares (corner-to-corner) are varied from 100 to 500 μm with an interval of 100 μm for optimization.

Using Buffered Hydrofluoric acid (BHF 5:1) and acetone as etchant unexposed SiO_2 layer and PPR layer were removed completely as shown (in steps 6 and 7 in Fig. 3). Then, TMAH etching was made uniformly on the patterned Si wafer. Initially, the etching was made for 30 min to optimize the etch rate, temperature and to monitor the microneedles shape. 45% TMAH solution with concentration of (10:0:0) was taken for etching the microneedles, but does not have sharp tips in the optimized temperature of 90 °C as shown in Fig. 5. Hence, the etching process was carried out with various concentrations and found that TMAH: Deionized (DI) water: Isopropyl Alcohol (IPA) (1:8:1) concentration gives better results in the growth and shape control of the microneedles. The optimized optical mask window size of 500 μm is chosen with center to center spacing between lateral and vertical directions and to

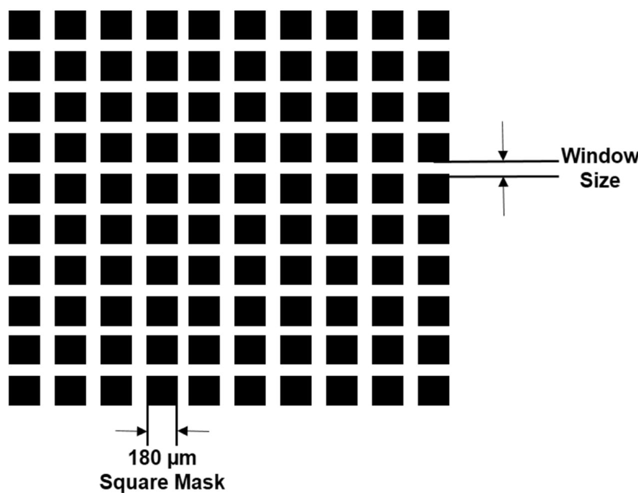

Fig. 2 Mask design for solid Si microneedles

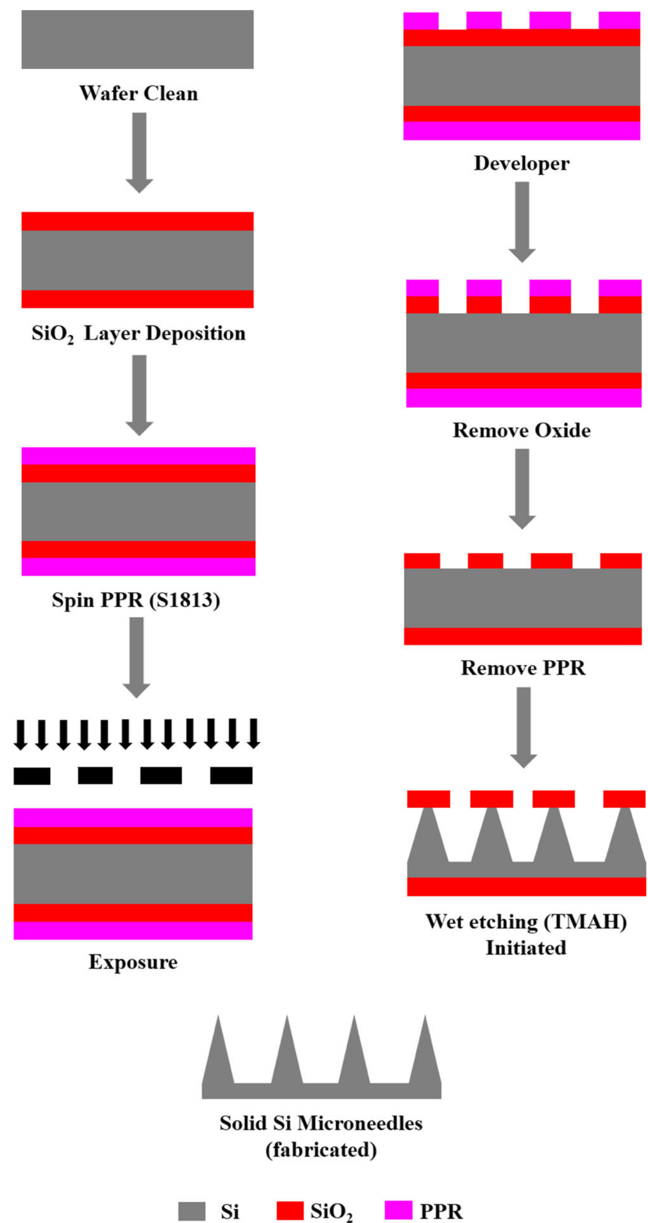

Fig. 3 Step by step process flow to fabricate solid Si microneedle array

counterpart the etch rate of lateral over vertical by producing an adequately smooth surface of microneedles. The concluding step of the experimental part was made to get the microneedle array during the fabrication using an optimized TMAH etching factors. Comparing needle height, base width, tip radius, angle and aspect ratio optimality of microneedles are measured. Finally, an array of solid silicon microneedles with a height of 158 μm was fabricated and shown in Fig. 9.

2.3 Hardness and mechanical strength

In order to estimate the mechanical strength of the microneedles, hardness test was carried out using the Vickers hardness tool. The diamond indenter is used to measure the hardness by applying a load of 25 gf with dwell time of 15 s as shown in Fig. 14. Hardness values of other materials are also recorded and compared to know the mechanical strength of the fabricated microneedles. It helps to avoid any further damages during penetration through skin to deliver drugs in TDDS applications.

2.4 Characterization

The oxide layer thickness was measured by using Sentech Ellipsometer (SE 800). Ambios XP–2 Surface Profilometer is used to obtain the surface profiles with its roughness, step height, etch depth and stress analysis of the PPR S1813, coated over the oxide layer. The morphology images are observed using by Zeiss Ultra 55 FE-SEM with Oxford EDX system where the elemental analysis of the microneedles is observed with a higher resolution of 1.2 nm @ 15 KV. Acceleration voltage (V_{acc}) used was 5 KV and the sample holder was tilted up to 45° angle to see the exact growth size, i.e. microneedles height. The surface profile parameters and topological characteristics are observed using Park Systems–NX10 Atomic Force Microscopy (AFM) operated in non-contact mode. FTIR spectra for all samples are collected using Thermo Scientific Nicolet IS5 Spectrophotometer in the range of 4000 cm^{-1}–600 cm^{-1}. UV-Vis-NIR studies are carried out in 200–2500 nm range using JASCO UV-Vis-NIR (Model–V–670) Spectrophotometer. Vickers hardness study is carried using Matsuzawa Vickers (Model–MMT–78B, Japan) hardness tool to measure the mechanical strength of the fabricated solid silicon microneedles.

3 Results and discussion

3.1 Thickness measurements of oxide layer and PPR

To measure the thickness and uniformity of oxide layer, three different Si wafers are taken at room temperature. Nine different spots over the wafer are taken into account to measure the uniformity and thickness of oxide grown using ellipsometry. For this, wavelength ranging from 240 to 930 nm is taken by keeping the angle at 70°. The average of thickness value observed for the oxide layer is 1 μm and the same is shown clearly in Fig. 4a.

PPR S1813 is spin coated over the oxide layer and its distribution with its thickness is measured using stylus profilometry. The surface of the layer is touched physically by the stylus profiler at five different spots over three different wafers. The vertical gesture is then converted into electrical signals which signifies surface topography. The samples may get damaged due to the physical contact between the stylus and the surface, while taking step height (average thickness obtained is 2 μm). The measured values for all three wafers are shown in Fig. 4b. Measurements made randomly on the wafers are shown inside both the figures.

3.2 Etching made before optimization

An anisotropic TMAH etching was carried initially for 30 min to find the shape of the microneedles as examined in Fig. 5a Figure 5b shows 7 × 7 arrays of solid silicon microneedle with the etching made using 25 wt.% concentrated TMAH solution of 180 mL i.e., TMAH:DI:IPA (10:0:0) solution. After etching for 1 h in the same TMAH concentration, single microneedle with an oxide layer captured is shown in Fig. 5c. The etch rate calculated here is 0.6 μm/min. Further, the etching process is carried out for 4 h and this gives the microneedle, a height of 136.1 μm but without sharp tips (Fig. 5d). Depending on the skin hardness and material chosen for the microneedles, it is easy to vary the needle height and sharpness of the tips. The major criterion is that the microneedles should cross the skin barrier without any damages. To achieve that, we initiated an optimized TMAH concentration to continue the fabrication with the available facilities.

3.3 Effects of TMAH etching factors

The determination of TMAH characterization tests are to achieve the etching factors, which can produce adequately smooth surface by controlling the vertical etch rate over its lateral equivalent as shown in Fig. 6. To set each constraint, 9 samples were prepared for each of the subsequent tests. Their average value is considered in the final optimization. For analyzing the influence of TMAH concentration over the microneedles shape, 10 compositions of TMAH taken from 10 to 100%, DI water drawn from 0 to 90% and IPA of 0% is fixed. Consequently, to investigate the effect of IPA, 9 compositions of TMAH taken from 10 to 90%, DI water drawn from 10 to 80% and IPA of 10% is equipped. In the significance of the active etching regions, two sets of experiments are chosen. During each experiment, a 180 mL TMAH solution is

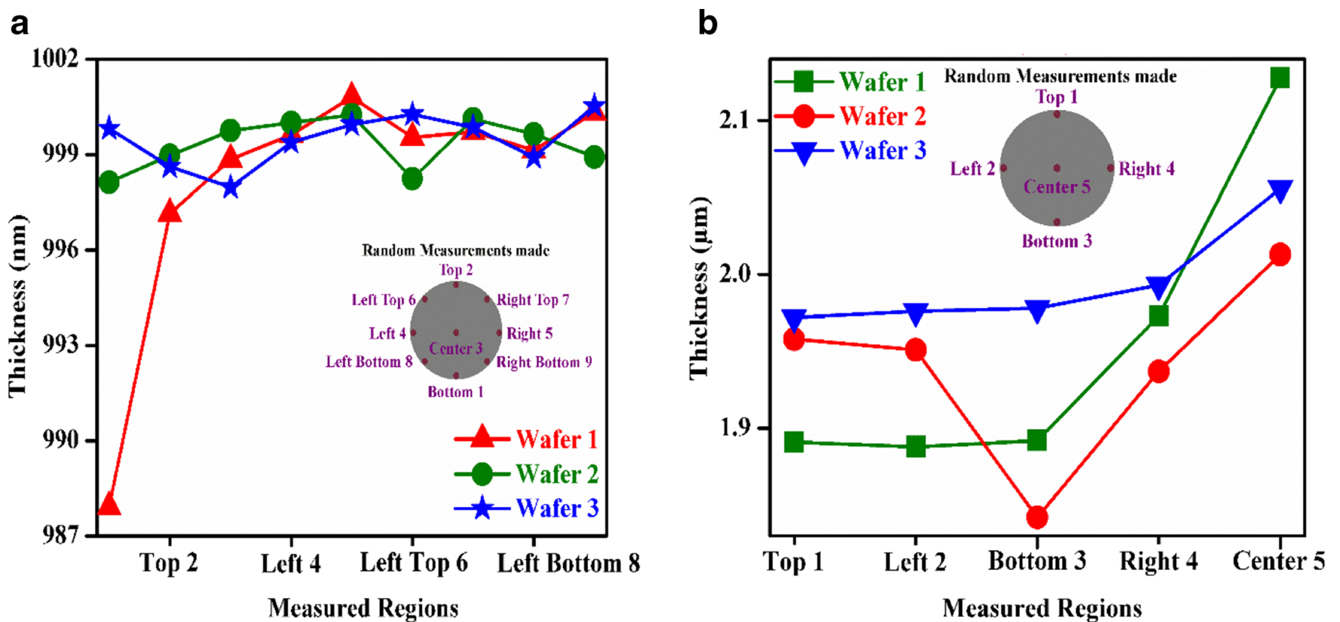

Fig. 4 Measured **a** SiO_2 layer thickness and **b** PPR thickness

used at 70 °C. Samples with an array of squares having 180 µm (length and width) with an interval of 100 µm are placed perpendicularly in the glass boat of TMAH setup. Detection of etch rate is made at intervals, changing among 5 and 30 min subjecting to the intensity of the etching method.

In other formalization tests, TMAH solution having a volume in the ratio of (TMAH: DI: IPA) 1:8:1 is used. This composition of TMAH produces a smooth surface profile and a desirable etch rate. For the interest of finding the optical mask window size effects, a group of 5 samples, having square arrays of 180 µm diameter, with spacing of 100, 200,

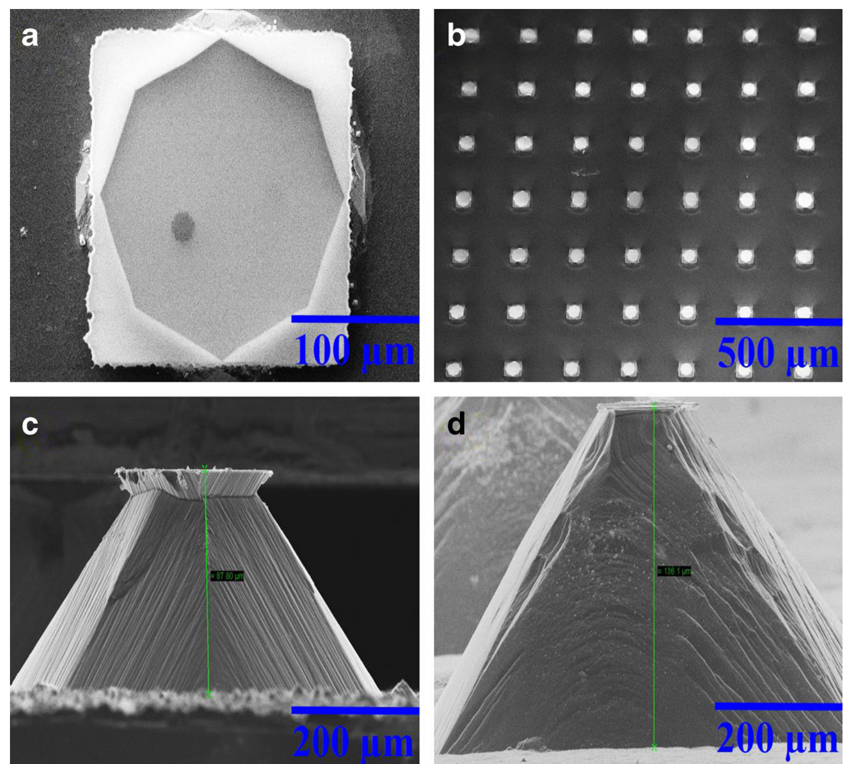

Fig. 5 **a** A hexagonal base formed in single solid Si microneedle. **b** 7 × 7 array of solid Si microneedles. **c** V-groove shape of solid Si microneedle with its oxide layer. **d** Finally obtained single solid Si microneedle (after 4 h etching)

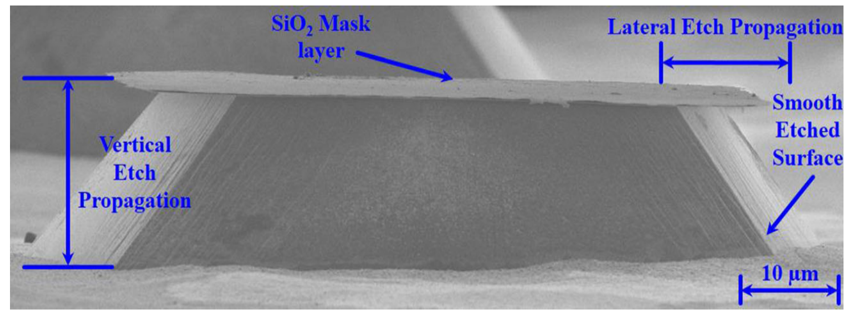

Fig. 6 Examination of vertical vs lateral etch transmissions

300, 400, and 500 µm are kept together in the glass boat of TMAH setup and etched for 5 min at a time into a 200 mL TMAH (1:8:1) solution. Later, the samples are rinsed in DI water and dried by blowing nitrogen air and studied under SEM for the occurrence of etching on both vertical and lateral directions. While analyzing the etching temperature effects over the microneedle surface profiles, 180 µm diameter squares with spacing of 100 µm arrays of samples are dipped in 180 mL TMAH (1:8:1) solution for 30 min. Variation with temperatures are tested at 70, 75, 80, 85, and 90 °C, respectively. To study the variations of etching propagation occurred in vertical and lateral directions, samples are examined using SEM. The samples are placed perpendicularly in the glass boat to control the maximum effect of lateral over vertical etch rate difference and to get a smooth surface profile. Finally, optimized etching factors are considered for the experimental side, along with TMAH concentration tests performed earlier, while fabricating solid silicon microneedles. The needle height, base tip, tip angle, tip diameter, and its aspect ratio are also calculated with these factors.

Measurements made on vertical and lateral directions of etching for numerous TMAH concentrations having 0 and 10% IPA are illustrated in Table 2. Concentrations of TMAH significantly affect the etch rates of silicon, which might be considered from the table. After making a close analysis, it exposed that not only concentration plays a prominent part in influencing the overall etch rate, there is an eventual difference in lateral and vertical etchings on varying TMAH concentration. The examined values are briefed in the last column of the Table 2. It clearly shows that for all TMAH concentrations examined, the percentage difference between vertical and horizontal etch rates are less than 7%, which shows the identical etching propagation in both directions. To plot the graph only vertical etch values are considered because both in lateral and vertical directions etching occurs uniformly, but vertical etch rates are the comparatively dominating ones. However, etch rates are considerably lower as masks patterned with a square window array are used in this work. The chosen mask

Table 2 Tested various TMAH concentrations with its vertical and lateral etch rates of patterned Si

Sl.no	TMAH: DI: IPA (vol. ratio in %)	Vertical etch rate (µm/min)	Lateral etch rate (µm/min)	Difference %
1.	100:0:0	0.59	0.63	−6.78
2.	90:10:0	0.64	0.65	−1.56
3	80:20:0	0.68	0.70	−2.94
4.	70:30:0	0.73	0.78	−6.85
5.	60:40:0	0.82	0.815	0.61
6.	50:50:0	0.84	0.82	2.38
7.	40:60:0	0.87	0.83	4.60
8.	30:70:0	0.91	0.88	3.30
9.	20:80:0	0.94	0.90	4.26
10.	10:90:0	0.96	0.93	3.13
11.	90:0:10	0.49	0.51	−4.08
12.	80:10:10	0.62	0.64	−3.23
13.	70:20:10	0.68	0.67	1.47
14.	60:30:10	0.78	0.71	5.46
15.	50:40:10	0.82	0.77	6.10
16.	40:50:10	0.85	0.80	5.88
17.	30:60:10	0.88	0.87	1.14
18.	20:70:10	0.93	0.95	−2.15
19.	10:80:10	0.96	0.92	4.17

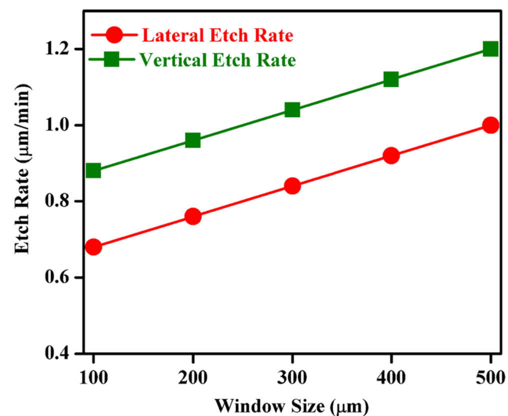

Fig. 7 Etch rates vs optical mask window size of 1:8:1 (TMAH:DI:IPA) solution at 70 °C

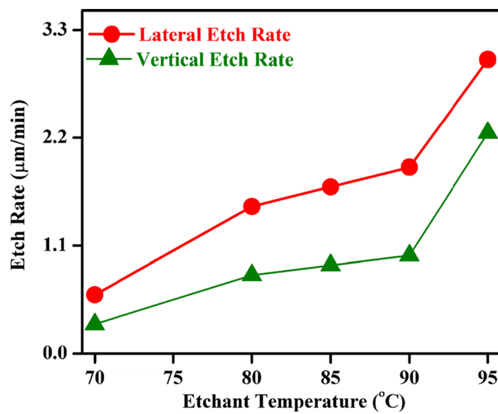

Fig. 8 Etch rates vs etchant temperature of 1:8:1 (TMAH:DI:IPA) solution

pattern has considerably slowed down the TMAH etching processing by dropping the mass transfer rates and ionic supply consequently keeping the etch rates low. On the other hand, distribution of etch rate is unique and high, due to the percentage of DI water added.

TMAH concentration ratio of 1:8:1 solution is considered appropriate for microneedles fabrication because in spite of its low etch rate, the entire etching method can be controlled very well, and the smoothing surface can result at this etchant concentration. This confirms that the TMAH initiation made uniformly over the exposed silicon surface begins rapidly as the sample is kept in the TMAH setup. As a result, etching through the surface begins at random areas generating no uniformity in surface morphology. An interesting phenomenon is observed when the spacing between the squares on the optical mask are varied by keeping the other factors constant. While increasing the window size, it is found that etch rates in both the vertical and lateral directions increase uniformly, but separately as shown in Fig. 7. The advantage of having a bigger window size gives the result of increasing the involved reactants mobility and availability. To increase the etch rate extremely, increasing the window size alone is not a factor, as there is a limit exists to the reactants' surface mobility. Our concern here is that the window size should not go beyond greater than 500 µm. As the needle gap becomes larger it leads to inappropriate design for microneedle array.

Not only the spacing between needles alone controls the etch rates in vertical and lateral directions, but also etching temperature plays a phenomenal role in it. Temperature delivers the required energy to the reactive elements, where it loosens its atomic bonds on the surface of the silicon. Consequently, it dissolves the silicon dioxide resulted in higher etch rate. Etch rates in vertical and lateral directions are increases separately and steadily up to 75 °C. Here, lateral etch rates are dominating compared to vertical etch rate and beyond this temperature level, both the etch rates increases drastically as shown in Fig. 8. Care is taken

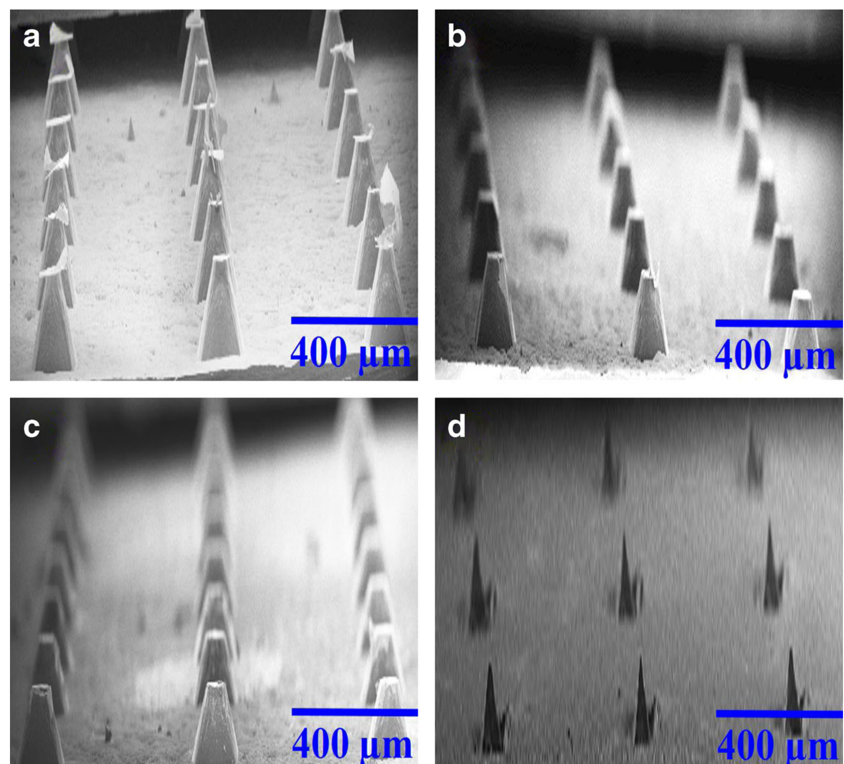

Fig. 9 **a** 3 × 6 array of solid Si microneedles with a SiO_2 layer. **b** Partially removed SiO_2 layer. **c** Fully removed SiO_2 layer. **d** Final solid Si microneedles (after 2 h 45 min etching)

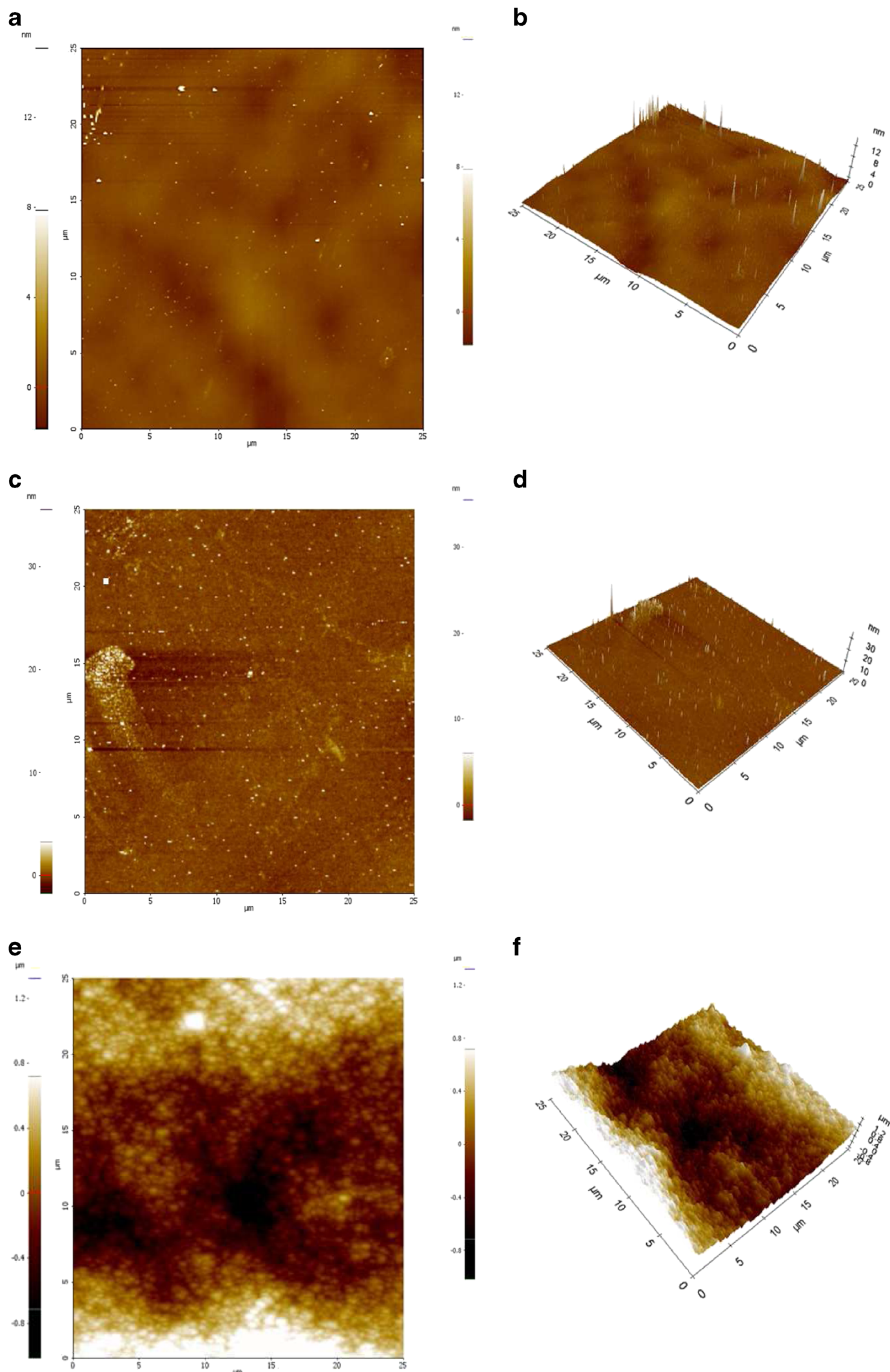

Fig. 10 AFM images at 25 × 25 μm scan range of 2D and 3D **a** and **b** Bare Si wafer. **c** and **d** SiO_2 grown over Si wafer. **e** and **f** Fabricated solid Si microneedle

here to slow down the lateral etching rate to obtain a uniform etching reaction. When temperature was raised above 90 °C, microneedles are slightly biased, signifying destructive rapid etching on the vertical side. SiO_2 mask layers are vanished completely in some areas due to severe reaction occurred at a high etchant temperature. Since etching evolves in both vertical and horizontal directions, we observed the significance that lateral surfaces in deep become less reachable by adding new etchants compared to its vertical parts. Increase in temperature supplies activation energy which stimulates freer moving particles in bulk. These are in closer immediacy to the etched surfaces in vertical.

3.4 Optimized parameters for solid Si microneedles fabrication

In our study after further examination, we have achieved sharper tip of microneedles by taking an optimized TMAH concentration as 1:8:1 of 180 mL solution. It was carried fully for the final anisotropic etching with its optimized etch rates. Figure 9a shows the solid silicon microneedles formed with an oxide layer at their tips. BHF etchant is used to remove the top oxide at the tips which is shown in Fig. 9b, c. The entire process of etching with all optimized factors is carried out fully for 2 h 45 min over the freshly patterned Si wafer to get sharper tips with lengthy microneedles. The etch rate calculated here is 0.96 μm and this gives the microneedle, the height of 158 μm. It is possible to get more height and sharper tips of microneedles by increasing the etching time. However, we stopped the etching process at 2 h 45 min because of not having the desired oxide layers and found broken wafers. It is observed from Fig. 9d that the fabricated solid silicon microneedles have a high aspect ratio with sharper tips.

The surface topography of both 2D and 3D of the bare Si wafer, SiO_2 layer grown and fabricated solid Si microneedles (exactly at the square window opening) are analyzed using AFM. Here, the scanning size is carried out in 25 × 25 μm as shown in Fig. 10. The dense morphology depicts the pores of Si whereas the surface topography shows continuous and fine grained microstructure with smooth surface on it. The entire oxide layer is dense and homogeneously grown with some peaks. Crystal grains grown uniformly for oxide layer during the oxidation process are observed from this AFM image with proper spacing. As far as the growth mode transition is considered, with the increased time in the furnace, the strain in the grains increases. This increase in roughness is attributed due to the height of oxide peaks which increases with an increase in the height difference between peaks and valleys of the grain size. The measurements are made in the center area to avoid edge effects of the oxide layer. Due to change in height and diameter of the microneedles, we could not observe the exact topography, but gives an evidence that wafer got etched and observed changes in surface roughness profile. Pores dispersed within the layer of the smooth surface are shown in the images. They are homogeneous in nature and grains are aligned on the etched Si wafer, i.e., microneedles. Table 3 illustrates the surface profile parameters observed for bare Si wafer, SiO_2 layer, and solid Si microneedles as the variations of RMS roughness (Rq) values, the variations of average roughness values (Ra), ten-point mean height (Rz) values, skewness of the line (Rsk), and kurtosis of the line (Rku). Skewness (Rsk) is the third moment of profile amplitude probability density function, which is negative here, showing that the surface is more planar and predominant valleys correspond to profile symmetry. Kurtosis (Rku) is the fourth moment of profile amplitude probability function measuring the surface sharpness, which is higher than 3 here, which means that the wafer has more peaks than valleys for both bare Si and SiO_2 layer, but for solid Si microneedles (Rku) value lower than 3 shows that the surface is flat and called as Platkykurtic.

3.5 Optical properties of fabricated microneedles

FTIR spectra of solid Si microneedles with a combination of Si and SiO_2 (various vibrations types) are illustrated in Fig. 11 and the assignment is given in Table 4. The spectrum is obtained by detecting the changes in transmittance (T) intensity as a function of frequency. Transmittance ranges from 0 to 100% T, where it provides better contrast between intensities of strong and weak bands in the spectra. The FTIR spectrum exhibits a peak at ~617 cm^{-1} due to the bulk Si–Si absorption/Si–O (out of plane vibration). A weak absorption exhibits at ~720 cm^{-1} in 600–800 cm^{-1} corresponds to the Si–H bending mode (rocking). Between 800 cm^{-1} and 1000 cm^{-1}, various

Table 3 Surface profile parameters for bare Si wafer, SiO_2 layer and solid Si microneedles

Samples	Rq nm	Ra nm	Rz nm	Rsk	Rku	(XEI Software) nm
Bare Si wafer	0.44	0.19	15.42	-3.71	65.61	12
SiO_2 layer	0.57	0.27	22.50	-1.14	6.42	16
Solid Si microneedles	370	300	2230	-0.351	2.68	1200

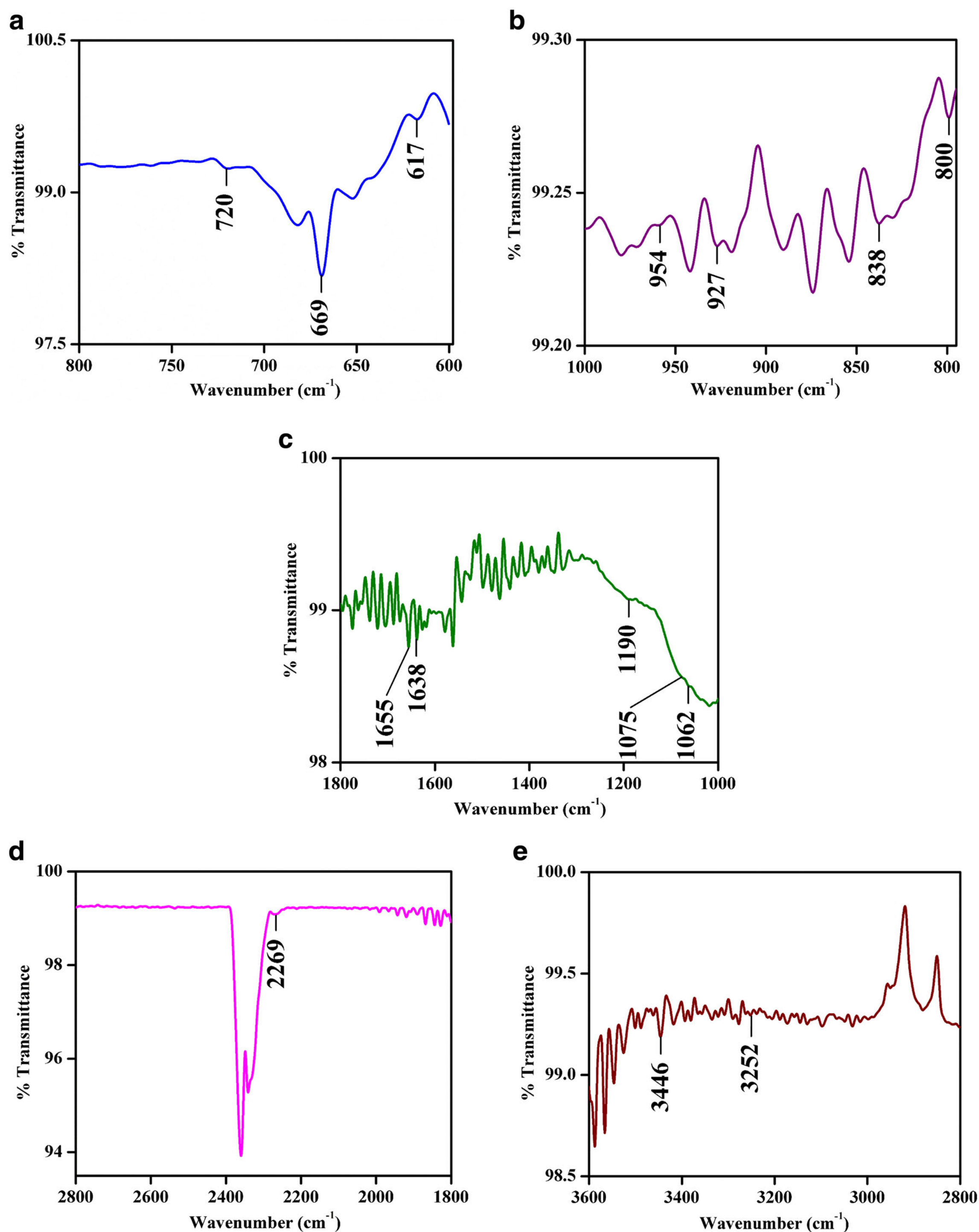

Fig. 11 FTIR spectra of Solid Si microneedles. **a** 600–800 cm^{-1}. **b** 800–1000 cm^{-1}. **c** 1000–1800 cm^{-1}. **d** 1800–2800 cm^{-1}. **e** 2800–3600 cm^{-1}

absorption modes appear, such as the Si–O–Si bending, Si–H bending, Si–OH, $Si–H_3$ deformation. With that, 800 cm^{-1} corresponds to an inter-tetrahedral Si–O–Si bending vibration mode and 954 cm^{-1} can be assigned to silanol groups (Si–OH mode). When we observed between 1000 to 1800 cm^{-1}, the transmission spectra showed peaks at 1062 cm^{-1} corresponding to Si–O stretching frequency. The band almost at 1085 cm^{-1} slightly shifted to 1075 cm^{-1} shows the presence of silicon dioxide, which is stoichiometric in structure and the band corresponds to Si–O–Si antisymmetric stretching vibrations. The 1638 cm^{-1} band occurred due to the bending vibration of H_2O molecules and at 1655 cm^{-1} associated with H–

Table 4 The assignment of functional groups from FTIR spectra of solid Si microneedles

Peak Position (cm^{-1})	Assignment	Origin nature
617	Si–O (out of plane vibration)	Medium absorption peak
720	Si–H bending vibration (rocking mode)	Weak absorption peak
800	Inter-tetrahedral Si–O–Si bending vibration	Strong Absorption Peak
954	Silanol groups (Si–OH mode) bending vibration.	Weak absorption peak
1062	Si–O stretching	Weak absorption peak
1075	Si–O–Si antisymmetric stretching	Weak absorption peak
1638	Bending vibration of H_2O	Strong absorption peak
1655	...–OH stretching	Strong absorption peak
2269	Si–O stretching	Medium absorption peak
3252	Si–OH stretching	Medium absorption peak
3446	...–OH stretching	Strong absorption peak

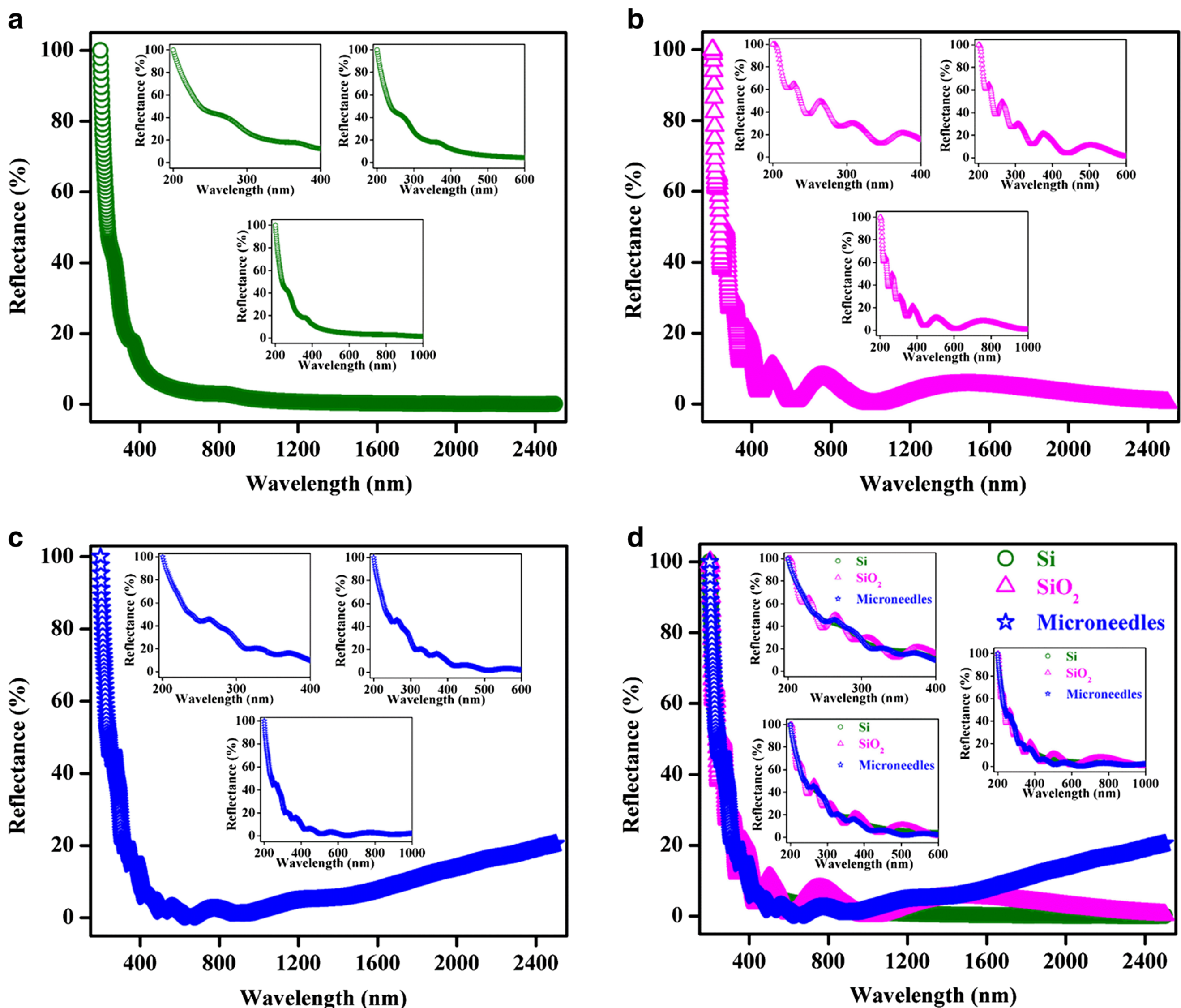

Fig. 12 The reflection spectra of **a** Bare Si wafer, **b** SiO_2 layer, **c** Solid Si microneedles, and **d** combined one

O–H (H_2O). 2269 cm^{-1} band observed from 1800 to 2800 cm^{-1} belongs to the Si–O stretching frequency. The transmission spectra shows the stretching vibrations of Si–OH groups observed at 3252 cm^{-1} corresponds to amorphous SiO_2 and the stretching vibration of H_2O molecules at 3446 cm^{-1} between 2800 to 3600 cm^{-1}. The vibrations are due to carbon impurity atoms in the spectral range (doublet at 2360 cm^{-1}, around of 1600 cm^{-1}, and sharp peak at 669 cm^{-1}). However, the functional groups in the Si microneedles which show no limitations to the optical properties are studied here. These results supported the wet etching carried at 90 °C, without affecting the properties of silicon to form solid Si microneedles [49, 50].

A preliminary test of the uniformity is done using UV–Vis–NIR spectroscopy in the range of 200–2500 nm. In Fig. 12, the reflection spectra of the three samples (i.e., Bare Si wafer, SiO_2 layer, and Solid Si microneedles) are shown, where the reflection intensity at an angle of 45 degree is for bare Si wafer, 60 degree for SiO_2 layer, and 46 degree for solid Si microneedles Due to average dimensions of holes etched on the surface, the relative intensity got decreased in lower wavelengths. Diffused light intensity data on the Si layer contains the signature of its morphology. The dimension and geometry of the holes etched on Si surface can be related with light scattering data in the range of 200–1000 nm (i.e., 200–400 nm, 200–600 nm, and 200–1000 nm separately) as shown in the inner images. The SiO_2 layer having uniform thickness is the observed result. Solid silicon microneedles are etched uniformly by keeping Si wafer as reference and its angle decreases compared to SiO_2 layer.

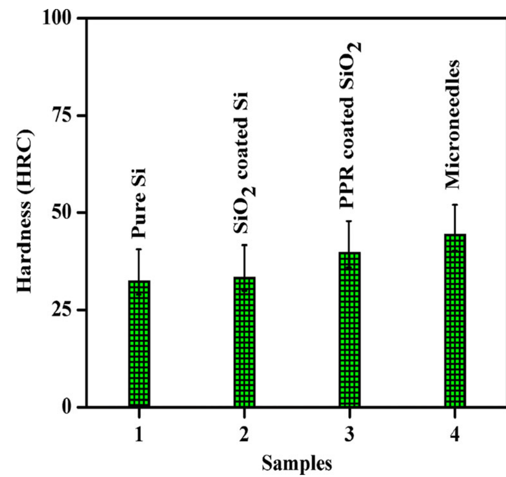

Fig. 14 Vickers hardness test measured and compared for solid Si microneedles

3.6 Elemental analysis and mechanical strength

Elemental analysis is used to characterize the elements present in the solid Si microneedles. Figure 13. confirms that no other elements other than silicon are present after the fabrication. Fabricated solid silicon microneedles can be used to deliver the drugs coated at their tips as it is. It can also be used as a sensory probe to measure the glucose level by extracting blood from the body.

The Vickers hardness test results of all samples, including bare Si wafer, SiO_2 grown layer, PPR S1813 coated one, and the fabricated solid Si microneedles are tested. Figure 14 gives

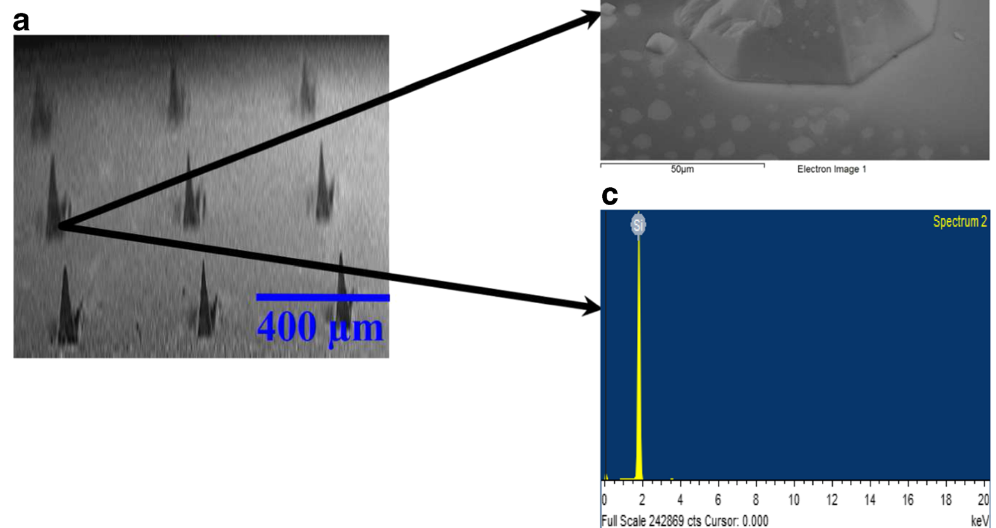

Fig. 13 Fabricated **a** solid Si microneedles, **b** single microneedle zoomed in to take EDX, and **c** EDX spectrum taken from single microneedle tip

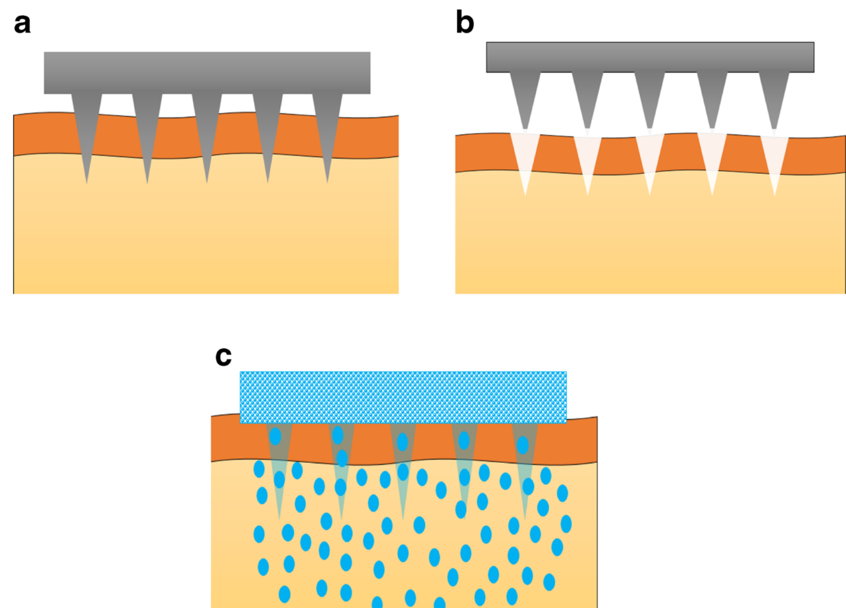

Fig. 15 Schematic view of the fabricated solid Si microneedles **a** during skin penetration, **b** impression after its drug delivery, and **c** delivered drug molecules

the comparison of the results. The Vickers hardness (HRC) value got increased after each layer adds one by one. Here, the hardness value (HRC) for solid Si microneedles is found to be 44.4 which gets increased by 36.7%, while compared with bare Si wafer whose hardness value (HRC) is determined as 32.5. The hardness of SiO_2 grown layer and PPR S1813 coated one showed a similar increment of 2.8 and 22.7%, respectively as compared with bare Si wafer hardness value. The hardness, H is evaluated by

$$H = \frac{P\max}{A} \tag{2}$$

where *Pmax* is the maximum applied load and *A* is the contact area of the indentation at the maximum load [51, 52]. Dwell time kept for all the calculations is 15 s. D_1 and D_2 are the arithmetic mean of the two diagonals, i.e., 12.5 μm. The Ultimate Tensile Strength (UTS) value of the skin predicted by Gallagher AJ et al. is 27.2 ± 9.3 MPa, taken as a reference here [53]. The obtained hardness value is in HRC, but the skin mechanical strength is mainly available in UTS values, Young's modulus values, etc. So, we preferred UTS value and to convert HRC values in that form, we used hardness conversion charts and calculator available on the web [54]. The UTS value for HRC 44.4 is 1420 MPa (N/mm^2). Compared to the referred UTS value, it shows clearly that fabricated microneedles are 52.2 times higher than the skin UTS value. For silicon microneedles, the mechanical strength is one of the important parameters during skin penetration either to deliver drugs or to extract blood for glucose measurements. Further, the biocompatibility gets improved by coating metals at the tip to deliver drugs by ensuring its strength to penetrate without causing any damage to the nerves and skin structures. Finally, fabricated solid silicon microneedles with its process during drug delivery is illustrated as schematic view in Fig. 15.

4 Conclusions

Fabrication of solid silicon microneedles with high aspect ratio is made using the optimized and characterized TMAH etching factors. This is a simple and cost effective approach. From AFM imaging, it is inferred that the optimized TMAH concentration did not affect the vertical to lateral etching ratio. In turn, it has well controlled topography at the etched part. Addition of IPA to the concentric region made the flat surface for the microneedles grown with a proper height and sharper tips. Etching factors are optimized for the TMAH concentration of 1:8:1 solution. The optical mask window size is directly proportional to TMAH etch rate, where the mobility rate of surface ions gets increased in the exposed area when the window size increases. Optimized etching temperature is 90 °C. Until that time, there was a variation in etching temperature that led to adverse conditions. To fabricate the solid silicon microneedles with a high aspect ratio, the surface of the sample placed in the glass boat should be kept perpendicular to the TMAH etching direction. Solid silicon microneedles with an average height of 158 μm, base width of 110.5 μm, having an aspect ratio of 1.43, tip angle of 19.4°, and tip diameter of 0.40 μm are obtained successfully. The mechanical stability tested using the Vickers hardness test for the fabricated microneedles satisfied the requirements. The obtained hardness value is higher and sufficient one to penetrate into the skin. Now, it becomes easy to insert microneedles without the possibility of fracture. For the sensory probe purpose,

fabricated needles are tested with its optical properties using FTIR and UV-Vis-NIR spectroscopies, respectively.

Acknowledgements The authors acknowledge the support provide by the Indian Nanoelectronics Users Programme (INUP)—IIT Bombay (IITB), India to carry this work and also thank CEN—(Centre of Excellence in Nano Technology), IITB for their permission to use the facilities. The authors also acknowledge the Ministry of Human Resource Development (MHRD), Government of India for the AFM, FTIR and UV-Vis-NIR spectroscopy facilities under the plan fund sanctioned to the Department of Physics, National Institute of Technology, Tiruchirappalli (NITT). One of the authors thank Dr. S. P. Kumaresh Babu, Associate Professor/HoD, Department of Metallurgical and Materials Engineering, NITT for providing Vickers hardness facilities.

References

1. Prausnitz MR (2004) Microneedles for transdermal drug delivery. Adv Drug Deliv Rev 56:581–587
2. Prausnitz MR, Langer R (2008) Transdermal drug delivery. Nat Biotechnol 26:1261–1268
3. Guy RH, Hadgraft J (2003) Transdermal Drug Delivery. Marcel Dekker, New York
4. Williams A (2003) Transdermal and topical drug delivery. Pharmaceutical Press, London
5. Prausnitz MR, Mitragotri S, Langer R (2004) Current status and future potential of transdermal drug delivery. Nat Rev Drug Discov 3:115–124
6. Henry S, McAllister DV, Allen MG, Prausnitz MR (1998) Microfabricated microneedles: a novel approach to transdermal drug delivery. J Pharm Sci 87:922–925
7. Lin L, Pisano AP (1999) Silicon-processed microneedles. IEEE J Microelectromech Syst 8:78–84
8. Tao SL, Desai TA (2003) Microfabricated drug delivery systems: from particles to pores. Adv Drug Deliv Rev 55:315–328
9. McAllister DV, Wang PM, Davis SP, Park JH, Canatella PJ, Allen MG, Prausnitz MR (2003) Microfabricated needles for transdermal delivery of macromolecules and nanoparticles: fabrication methods and transport studies. Proc Natl Acad Sci U S A 100:13755–13760
10. Van der maaden K, Sekerdag E, Schipper P, Kersten G, Jiskoot W, Bouwstra J (2015) Layer-by-layer assembly of inactivated poliovirus and N-Trimethyl chitosan on pH-sensitive microneedles for dermal vaccination. Langmuir 31:8654–8660
11. Quan FS, Kim YC, Song JM, Hwang HS, Compans RW, Prausnitz MR (2013) Long-term protective immunity from an influenza virus-like particle vaccine administered with a microneedle patch. Clin Vaccine Immunol 20:1433–1439
12. Van der maaden K, Jiskoot W, Bouwstra J (2012) Microneedle technologies for (trans) dermal drug and vaccine delivery. J Control Release 161:645–655
13. Cormier M, Johnson B, Ameri M, Nyam K, Libiran L, Zhang DD, Daddona P (2004) Transdermal delivery of desmopressin using a coated microneedle array patch system. J Control Release 97:503–511
14. Park JH, Allen MG, Prausnitz MR (2005) Biodegradable polymer microneedles: fabrication, mechanics and transdermal drug delivery. J Control Release 104:51–66
15. Martanto W, Moore JS, Kashlan O, Kamath R, Wang PM, O'Neal JM, Prausnitz MR (2006) Microinfusion using hollow microneedles. Pharm Res 23:104–113
16. Bariya SH, Gohel MC, Mehta TA, Sharma OP (2012) Microneedles: an emerging transdermal drug delivery system. J Pharm Pharmacol 64:11–29
17. Van der maaden K, Luttge R, Vos PJ, Bouwstra J, Kersten G, Ploemen I (2015) Microneedle-based drug and vaccine delivery via nanoporous microneedle arrays. Drug Deliv and Transl Res 5: 397–406
18. McAllister DV, Allen MG, Prausnitz MR (2000) Microfabricated microneedles for gene and drug delivery. Annu Rev Biomed Eng 2: 289–313
19. Donnelly RF, Singh TRR, Woolfson AD (2010) Microneedle-based drug delivery systems: microfabrication, drug delivery, and safety. Drug Deliv 17:187–207
20. Kim YC, Park JH, Prausnitz MR (2012) Microneedles for drug and vaccine delivery. Adv Drug Deliv Rev 64:1547–1568
21. Pradeep Narayanan S, Raghavan S (2016) Transdermal drug delivery with tiny (micro) needles—an overview. South Asian Journal of Research in Engineering Science and Technology 1:378–387
22. Gill HS, Prausnitz MR (2007) Coated microneedles for transdermal delivery. J Control Release 117:227–237
23. Vrdoljak A, McGrath MG, Carey JB, Draper SJ, Hill AVS, O'Mahony C, Crean AM, Moore AC (2012) Coated microneedle arrays for transcutaneous delivery of live virus vaccines. J Control Release 159:34–42
24. Hegde NR, Kaveri SV, Bayry J (2011) Recent advances in the administration of vaccines for infectious diseases: microneedles as painless delivery devices for mass vaccination. Drug Discov Today 16:1061–1068
25. Cha KJ, Kim T, Park SJ, Kim DS (2014) Simple and cost-effective fabrication of solid biodegradable polymer microneedle arrays with adjustable aspect ratio for transdermal drug delivery using acupuncture microneedles. J Micromech Microeng 24:115015–115022
26. Hong X, Wei L, Wu F, Wu Z, Chen L, Liu Z, Yuan W (2013) Dissolving and biodegradable microneedle technologies for transdermal sustained delivery of drug and vaccine. Drug Des Deve Ther 7:945–952
27. LaVan DA, McGuire T, Langer R (2003) Small-scale systems for in vivo drug delivery. Nat Biotechnol 21:1184–1191
28. Hashmi S, Ling P, Hashmi G, Reed M, Gaugler R, Timmer W (1995) Genetic transformation of nematodes using arrays of micromechanical piercing structures. BioTechniques 19:766–770
29. Kaushik S, Hord AH, Denson DD, McAllister DV, Smitra S, Allen MG, Prausnitz MR (2001) Lack of pain associated with Microfabricated microneedles. Anesth Analg 92:502–504
30. Indermun S, Luttge R, Choonara YE, Kumar P, Toit LCD, Modi G, Pillay V (2014) Current advances in the fabrication of microneedles for transdermal delivery. J Control Release 185:130–138
31. Mikszta JA, Alarcon JB, Brittingham JM, Sutter DE, Pettis RJ, Harvey NG (2002) Improved genetic immunization via micromechanical disruption of skin-barrier function and targeted epidermal delivery. Nat Med 8:415–419
32. Martanto W, Davis SP, Holiday NR, Wang J, Gill HS, Prausnitz MR (2004) Transdermal delivery of insulin using microneedles in vivo. Pharm Res 21:947–952
33. Park JH, Choi SO, Seo S, Choy YB, Prausnitz MR (2010) A microneedle roller for transdermal drug delivery. Eur J Pharm Biopharm 76:282–289
34. Hamzah AA, Aziz NA, Majlis BY, Yunas J, Dee CF, Bais B (2012) Optimization of HNA etching parameters to produce high aspect ratio solid silicon microneedles. J Micromech Microeng 22:095017 (10pp)
35. Li WZ, Huo MR, Zhou JP, Zhou YQ, Hao BH, Liu T, Zhang Y (2010) Super-short solid silicon microneedles for transdermal drug delivery applications. Int J Pharm 389:122–129
36. Gill HS, Denson DD, Burris BA, Prausnitz MR (2008) Effect of microneedle design on pain in human subjects. Clin J Pain 24:585–594

37. Ji J, Tay FEH, Miao J, Iliescu C (2006) Microfabricated microneedle with porous tip for drug delivery. J Micromech Microeng 16:958–964
38. Wilke N, Hibert C, O'Brien J, Morrissey A (2005) Silicon microneedle electrode array with temperature monitoring for electroporation. Sens Actuators A Phys 123–124:319–325
39. Hanein Y, Schabmueller CGJ, Holman G, Lucke P, Denton DD, Bohringer KF (2003) High-aspect ratio submicrometer needles for intracellular applications. J Micromech Microeng 13:S91–S95
40. Lee JW, Park JH, Prausnitz MR (2008) Dissolving microneedles for transdermal drug delivery. Biomaterials 29:2113–2124
41. Chu LY, Choi SO, Prausnitz MR (2010) Fabrication of dissolving polymer microneedles for controlled drug encapsulation and delivery: bubble and pedestal microneedle designs. J Pharm Sci 99: 4228–4238
42. Sullivan SP, Koutsonanos DG, Martin MDP, Lee JW, Zarnitsyn V, Choi SO, Murthy N, Compans RW, Skountouz I, Prausnitz MR (2010) Dissolving polymer microneedle patches for influenza vaccination. Nat Med 16:915–920
43. Migalska K, Morrow DIJ, Garland MJ, Thakur R, Woolfson AD, Donelly RF (2011) Laser-engineered dissolving microneedle arrays for transdermal macromolecular drug delivery. Pharm Res 28: 1919–1930
44. Garland MJ, Salvador EC, Migalska K, Woolfson AD, Donelly RF (2012) Dissolving polymeric microneedle arrays for electrically assisted transdermal drug delivery. J Control Release 159:52–59
45. McCrudden MTC, Alkilani AZ, McCrudden CM, McAlister E, McCarthy HO, Woolfson AD, Donelly RF (2014) Design and physicochemical characterisation of novel dissolving polymeric microneedle arrays for transdermal delivery of high dose, low molecular weight drugs. J Control Release 180:71–80
46. Lahiji SF, Dangol M, Jung H (2015) A patchless dissolving microneedle delivery system enabling rapid and efficient transdermal drug delivery. Sci Rep 5:7914 (1–7)
47. Mistilis MJ, Joyce JC, Esser ES, Skountouz I, Compans RW, Bommarius AS, Prausnitz MR (2016) Long-term stability of influenza vaccine in a dissolving microneedle patch. Drug Deliv and Transl Res. doi:10.1007/s13346-016-0282-2
48. Chen YT, Hsu CC, Tsai CH, Kang SW (2010) Fabrication of microneedles. J Mar Sci Tech Taiw 18:243–248
49. Music S, Vincekovic NF, Sekovanic L (2011) Precipitation of amorphous SiO_2 particles and their properties. Braz J Chem Eng 28:89–94
50. Matsui Y, Adachi S (2012) Optical properties of porous silicon layers formed by Electroless photovoltaic etching. ECS J Solid State Sci Technol 1:R80–R85
51. Oliver WC, Pharr GM (1992) An improved technique for determining hardness and elastic modulus using load and displacement sensing indentation experiments. J Mater Res 7:1564–1583
52. Sakharova NA, Fernandes JV, Antunes JM, Oliveira MC (2009) Comparison between Berkovich, Vickers and conical indentation tests: a three-dimensional numerical simulation study. Int J Solids Struct 46:1095–1104
53. Gallagher AJ, Anniadh AN, Bruyere K, Otténio M, Xie H, Gilchrist MD (2012) Dynamic tensile properties of human skin. IRCOBI Conference 59:494–502
54. Metrics M https://mdmetric.com/tech/hardnessconversion.html. Accessed 18 August 2016